10-10-2012

A Method For Localizing Energy Dissipation In Blazars Using Fermi Variability

Amanda Dotson

Markos Georganopoulos

Demosthenes Kazanas

Eric S. Perlman

The Astrophysical Journal Letters, 758:L15 (5pp), 2012 October 10 doi:10.1088/2041-8205/758/1/L15

A METHOD FOR LOCALIZING ENERGY DISSIPATION IN BLAZARS USING *FERMI* VARIABILITY

Amanda Dotson[1], Markos Georganopoulos[1,2], Demosthenes Kazanas[2], and Eric S. Perlman[3]
[1] Department of Physics, University of Maryland Baltimore County, 1000 Hilltop Circle, Baltimore, MD 21250, USA; adot1@umbc.edu
[2] NASA Goddard Space Flight Center, Code 660, Greenbelt, MD 20771, USA
[3] Department of Physics and Space Sciences, Florida Institute of Technology, 150 West University Boulevard, Melbourne, FL 32901, USA
Received 2012 July 31; accepted 2012 September 6; published 2012 September 21

ABSTRACT

The distance of a *Fermi*-detected blazar γ-ray emission site from a supermassive black hole is a matter of active debate. Here we present a method for testing if the GeV emission of powerful blazars is produced within the subparsec-scale broad-line region (BLR) or farther out in the parsec-scale molecular torus (MT) environment. If the GeV emission takes place within the BLR, the inverse Compton (IC) scattering of the BLR ultraviolet (UV) seed photons that produces the γ-rays takes place at the onset of the Klein–Nishina regime. This causes the electron cooling time to become practically energy-independent and the variation of the γ-ray emission to be almost achromatic. If, on the other hand, the γ-ray emission is produced farther out in the parsec-scale MT, the IC scattering of the infrared (IR) MT seed photons that produces the γ-rays takes place in the Thomson regime, resulting in energy-dependent electron cooling times, manifested as faster cooling times for higher *Fermi* energies. We demonstrate these characteristics and discuss the applicability and limitations of our method.

Key words: galaxies: active – gamma rays: galaxies – quasars: general – radiation mechanisms: non-thermal

Online-only material: color figures

1. INTRODUCTION

Blazars dominate the extragalactic γ-ray sky (Nolan et al. 2012), exhibiting flares in which the *Fermi* γ-ray flux is seen to increase the pre-flare level up to several times (e.g., Abdo et al. 2010a). Because the emitting regions are unresolved, the location of the GeV emission remains unknown and this constitutes an open issue in understanding energy dissipation in blazars.

In the leptonic model, the GeV emission of blazars is produced by inverse Compton (IC) scattering of photons off of the same relativistic electrons in the jet that give rise to synchrotron radiation (for a review see Böttcher 2007). The seed photons for IC scattering are synchrotron photons originating within the relativistic jet (synchrotron self-Compton, SSC, scattering; e.g., Maraschi et al. 1992) or photons originating external to the jet (external Compton, EC, scattering), such as UV accretion disk photons (Dermer et al. 1992), UV photons originating from the broad-line region (BLR; Sikora et al. 1994), and IR photons originating from the molecular torus (MT; e.g., Błażejowski et al. 2000).

Because the γ-ray emission of blazars can vary significantly on short times, down to the instrument limits, ranging from a few minutes (in the TeV range; Aharonian et al. 2009) to a few hours (in the GeV range; Foschini et al. 2011), light-travel time arguments constrain the size of the emitting region and it has been argued (e.g., Tavecchio et al. 2010) that this requires the emission to take place at the subparsec scale. Explaining the *Fermi* GeV spectral breaks seen in powerful blazars (Abdo et al. 2010c) as a result of pair absorption on the He Lyman recombination continuum and lines, produced in the inner part of the BLR, places the GeV emission well within the BLR (Poutanen & Stern 2010). Very short distances ($\lesssim 10^{16}$ cm), however, where accretion disk photons dominate are not favored because of the high pair production γ-ray opacity (e.g., Ghisellini & Tavecchio 2009).

Gamma-ray flares have been associated with radio and optical flares, placing the GeV emission outside the BLR; Lähteenmäki & Valtaoja (2003), using the temporal separation of the radio and γ-ray fluxes, argued that the γ-ray emission site is at a distance of $\sim$5 pc from the central engine. Connections have also been drawn between γ-ray outbursts, optical flare polarization changes, and ejections of superluminal radio knots on the parsec scale; Marscher et al. (2010) associated short γ-ray variations with the passage of disturbances from the radio core, parsecs away from the black hole. In the case of OJ 287, Agudo et al. (2011) found γ-ray flaring to be simultaneous with millimeter outbursts associated with a Very Long Baseline Array jet component 14 pc downstream from the radio core.

Here we propose a method to distinguish if the GeV emission of powerful blazars takes place within the subparsec BLR or farther out within the parsec-scale MT. In Section 2, we discuss our understanding of the BLR, MT, and SSC photon fields and where each one dominates. We show that cooling on the UV BLR photons results in achromatic cooling times in the *Fermi* band, while cooling on the MT IR photons results in faster cooling times at higher γ-ray energies. In Section 3, we present our method, discussing the dilution of an energy-dependent cooling time from light-travel time effects and discuss the applicability of our method. Finally, in Section 4 we present our conclusions.

2. COOLING OF GeV-EMITTING ELECTRONS

2.1. Characterizing the BLR and the MT

Reverberation mapping of the BLR points to a typical size of $R_{\rm BLR} \approx 10^{17}\, L_{d,45}^{1/2}$ cm (e.g., Kaspi et al. 2007; Bentz et al. 2009), where $L_{d,45}$ is the accretion disk luminosity in units of 10^{45} erg s^{-1}. Because of this scaling, and assuming that $L_{\rm BLR} = \xi_{\rm BLR} L_d$, where $\xi_{\rm BLR} \sim 0.1$ is the BLR covering factor, the energy density inside the BLR ($U_{\rm BLR} \sim 10^{-2}$ erg cm^{-3}) is not expected to vary widely from object to object (Ghisellini & Tavecchio 2009). As was shown by Tavecchio (2008), when transformed to the jet frame, the BLR spectrum, dominated by H Lyα photons, is broadened and boosted in luminosity due to relativistic effects and can be well approximated by a blackbody spectrum that peaks at $\nu_{\rm BLR} = 1.5\,\Gamma\,\nu_{\rm Ly\alpha}$ ($\epsilon_{\rm BLR} \approx 3 \times 10^{-5}\,\Gamma$), where Γ is the bulk Lorentz factor and ϵ is the photon energy in mc^2 units.

In the MT, the dust temperature ranges from $T \sim 300$ K (Landt et al. 2010) to $T \sim 1200$ K (Cleary et al. 2007; Malmrose et al. 2011), with hotter emitting material expected to be closer to the central engine (e.g., Nenkova et al. 2008). Because of the larger size of the MT, it has been probed by reverberation mapping only for Seyfert galaxies (e.g., Suganuma et al. 2006) which have lower luminosities and therefore smaller MT sizes. These studies, along with near-IR interferometric studies (e.g., Kishimoto et al. 2011), also support an $R \propto L_d^{1/2}$ scaling, suggesting that U is similar for sources of different luminosities. Adopting the scaling of Ghisellini & Tavecchio (2009), $R_{\rm MT} = 2.5 \times 10^{18} L_{d,45}^{1/2}$ cm, and assuming a covering factor $\xi_{\rm MT} \sim 0.1$–0.5, the MT photon energy density is $U_{\rm MT} \sim 10^{-4}$ erg cm^{-3}. We also adopt a temperature $T_{\rm MT} \approx 1000$, corresponding to a blackbody peak at $\nu_{\rm MT} \approx 6.0 \times 10^{13}$ Hz ($\epsilon_{\rm MT} \approx 5 \times 10^{-7}$).

2.2. Which Seed Photons Dominate Where?

For an isotropic photon field, the comoving (jet frame) energy density U' is $U' \approx (4/3)\Gamma^2 U$, while for photons entering the emitting region from behind, $U' \approx (3/4)\Gamma^{-2} U$ (Dermer & Schlickeiser 1994). If the emission site is located at $R \lesssim R_{\rm BLR}$, the BLR photon field can be considered isotropic in the galaxy frame and, using the BLR energy density discussed in Section 2.1, $U'_{\rm BLR} \sim 1.3 \times \Gamma_{10}^2$ erg cm^{-3}. Similarly, the MT photon field is isotropic inside the BLR and its comoving seed photon energy density is $U'_{\rm MT} \sim 1.3 \times 10^{-2}\ \Gamma_{10}^2$ erg cm^{-3}. Clearly, at $R_{\rm BLR}$ scales, $U'_{\rm BLR}$ dominates over $U'_{\rm MT}$ by a factor of $\sim$100. If the emission site is located at $R \sim R_{\rm MT}$, then the BLR photons enter the emitting region practically from behind, so that $U'_{\rm BLR} \sim 7.5 \times 10^{-7} \Gamma_{10}^{-2}$ erg cm^{-3}. The MT photons retain the same comoving energy density as before and, in this case, the MT dominates the comoving photon energy density.

These external photon field comoving energy densities need to be compared to the synchrotron one. If $R_{\rm blob}$ is the size of the emitting region, then the comoving synchrotron photon energy density is $U'_S \approx L_s/(4\pi c R_{\rm blob}^2 \delta^4)$, where δ is the usual Doppler factor and L_s the synchrotron luminosity. An upper limit to $R_{\rm blob}$ is set by the variability timescale t_v: $R_{\rm blob} \lesssim c t_v \delta/(1+z)$, where z is the source redshift. We then obtain a lower limit $U'_s \approx L_s (1+z)^2/(4\pi c^3 t_v^2 \delta^6)$ or $U'_s \sim 6.3 \times 10^{-2} L_{s,46} (1+z)^2 t_{v,1d}^{-2} \delta_{10}^{-6}$ erg cm^{-3}, where $t_{v,1d}$ is the variability time in days. Setting $\delta = \Gamma$ the condition $U'_s < U'_{\rm ext}$ requires

$$\Gamma \gtrsim \left(\frac{3 L_s (1+z)^2}{16\pi c^3 t_v^2 U'_{\rm ext}} \right)^{1/8} = 8.6 \left(\frac{L_{s,46} (1+z)^2}{t_{v,1d}^2 U'_{\rm ext,-4}} \right)^{1/8}. \quad (1)$$

This translates to $\Gamma \gtrsim 4.8 \times L_{s,46}^{1/8} (1+z)^{1/4} t_{v,1d}^{-1/4}$ for the emission site at $R_{\rm BLR}$ scales and $\Gamma \gtrsim 8.6 \times L_{s,46}^{1/8} (1+z)^{1/4} t_{v,1d}^{-1/4}$ for the emission site at $R_{\rm MT}$ scales. In general, powerful quasars exhibit superluminal motions requiring $\Gamma \sim$ 10–40 (Jorstad et al. 2005; Kharb et al. 2010), and therefore, the dominant source of seed photons for these sources should be the BLR or the MT, provided the γ-ray emission site is at a distance not significantly larger than the size of the MT. A recent finding by Meyer et al. (2012) that the ratio of γ-ray to synchrotron luminosity increases with increasing radio core, as expected for EC emission (Dermer 1995; Georganopoulos et al. 2001), further supports the possibility that powerful blazars are EC emitters.

2.3. Cooling in the BLR versus Cooling in the MT

The critical difference between the BLR and the MT is the energy of the seed photons: the BLR produces UV photons while the MT produces IR photons. This difference by a factor of $\sim$100 *in typical photon energy is critical in that it affects the energy regime in which the GeV-emitting electron IC cooling takes place, and thus the energy dependence of the electron cooling time.*

For this consideration to be relevant, IC cooling must dominate over synchrotron cooling. This condition is satisfied, since in powerful blazars the IC luminosity clearly dominates over the synchrotron luminosity, reaching in high states an IC luminosity higher than that of the synchrotron by a factor of up to $\sim$100 (e.g., Abdo et al. 2010b; Meyer et al. 2012).

For electrons cooling in the Thomson regime ($\gamma\epsilon_0 \ll 1$, where both the electron Lorentz factor γ and the seed photon energy ϵ_0 are measured in the same frame), the cooling rate $\dot{\gamma} \propto \gamma^2$. For electrons with $\gamma\epsilon_0 \gg 1$ cooling takes place in the Klein–Nishina (KN) regime with $\dot{\gamma} \propto \ln\gamma$ (Blumenthal & Gould 1970). For the broad intermediate regime, $10^{-2} \lesssim \gamma\epsilon_0 \lesssim 10^2$, a parametric approximation has been suggested (Moderski et al. 2005). In what follows we calculate numerically the electron energy loss rate $\dot{\gamma}$, which for monoenergetic seed photons of number density n_0 and dimensionless energy ϵ_0 is

$$\dot{\gamma} = n_0 \int_0^\infty \frac{3\sigma_T c}{4\epsilon_0} f(x)(\epsilon - \epsilon_0) d\epsilon, \quad (2)$$

where, following Jones (1968),

$$f(x) = 2x \log x + x + 1 - 2x^2 + \frac{(4\epsilon_0 \gamma x)^2}{1 + 4\epsilon_0 \gamma x}(1-x), \quad (3)$$

with $x = \epsilon/[4\gamma^2 \epsilon_0 (1 - \epsilon/\gamma)]$.

The effects of the transition between Thomson and KN regimes on the electron energy distribution (EED) and the resultant spectrum of the synchrotron and IC emission have been studied before (e.g., Blumenthal 1971; Zdziarski 1989; Dermer & Atoyan 2002; Sokolov et al. 2004; Moderski et al. 2005; Kusunose & Takahara 2005; Georganopoulos et al. 2006; Manolakou et al. 2007; Sikora et al. 2009).

In short, the transition from Thomson to KN cooling in the EED can be seen for the steady state $n(\gamma) \propto \int Q(\gamma) d\gamma/\dot{\gamma}$: for a power-law injection $Q(\gamma) \propto \gamma^{-p}$, the cooled EED hardens from $n(\gamma) \propto \gamma^{-(p+1)}$ in the Thomson regime to $n(\gamma) \propto \gamma^{-(p-1)}$ in the KN regime. The transition takes place gradually at $\gamma \sim \epsilon_0^{-1}$. A second transition back to $n(\gamma) \propto \gamma^{-(p+1)}$ is expected at higher γ, as synchrotron losses (assumed to be less significant than Thomson EC losses) become larger than KN losses. The imprint of these considerations on the observed synchrotron and IC spectra has been considered for the case of the X-ray emission of large-scale jets (Dermer & Atoyan 2002) and in the case of blazars (Kusunose & Takahara 2005; Georganopoulos et al. 2006; Sikora et al. 2009).

Spectral signatures, however, are not unique and can be diluted or altered by extraneous causes (e.g., the accelerated electron distribution has intrinsic features that deviate from a power law, the synchrotron emission is contaminated by the big blue bump, and the IC emission is modified by pair production absorption from synchrotron or external photons). For these reasons their use in understanding where the GeV emission takes place is problematic.

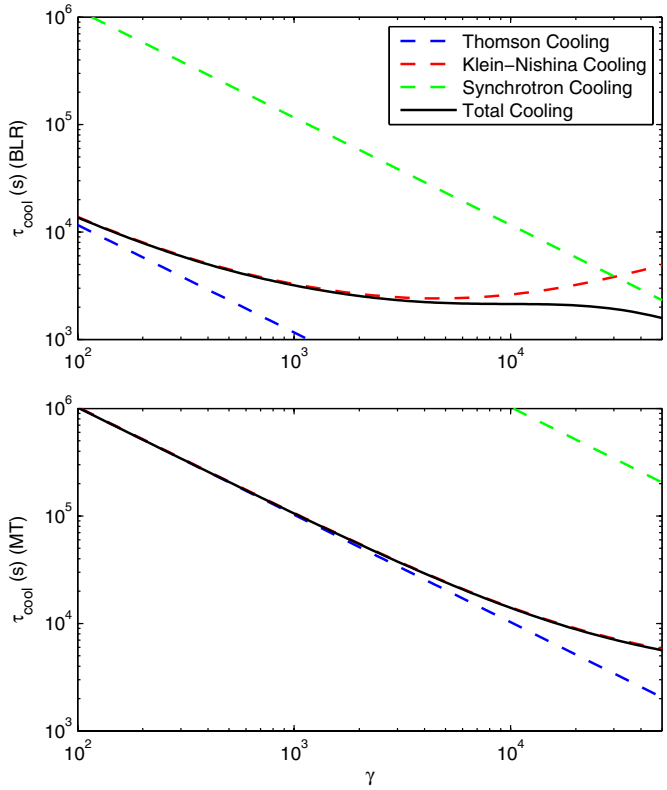

Figure 1. Electron cooling time in the galaxy frame as a function of γ. Top panel: blazar emission site located in the BLR. Bottom panel: blazar located in the MT. Broken lines represent the various cooling mechanisms and the solid black line is the total cooling time. Plots were calculated for seed photon energies $\epsilon_{0,\mathrm{BLR}} = 3\times10^{-5}$ and $\epsilon_{0,\mathrm{MT}} = 5\times10^{-7}$, seed photon energy densities $U_{\mathrm{BLR}} = 10^{-2}$ erg cm^{-3}, $U_{\mathrm{MT}} = 10^{-4}$ erg cm^{-3}, and magnetic field energy $U_B = 100\,U_{\mathrm{EC}}$.

(A color version of this figure is available in the online journal.)

3. LOCATING THE GeV EMISSION SITE

There is, however, another observable aspect of the Thomson–KN transition that is free of the issues faced by relying on spectral signatures: *the energy dependence of the electron cooling time can be used to evaluate the regime at which the electrons that produce the GeV radiation cool, and through this evaluate where the emission takes place.*

In the Thomson regime, the electron cooling time $t_c = \gamma/\dot{\gamma}$ scales as γ^{-1}, while in the KN regime the electron cooling time scales as $\gamma/\ln\gamma$. These two regimes connect smoothly, forming a wide *valley* around $\gamma\epsilon_0 \sim 1$ in which the cooling time is practically energy-independent. The energy of the seed photons originating in the BLR is greater than that of photons from the MT by a factor of ∼100. As a result, (see Figure 1) the location of the energy-independent valley of the BLR case is manifested at electron energies lower by a factor of ∼100 than that of the MT case. In turn, the energy dependence of t_c causes a related energy dependence in the observed falling time t_f of the flare. The falling time t_f of *Fermi* light curves can be used, therefore, to determine whether a flare occurs within the BLR or within the MT.

3.1. Flare Decay in the BLR versus Flare Decay in the MT

We utilize a one-zone code to demonstrate the effect of a flare occurring within the BLR versus a flare occurring within the MT. The code assumes the injection of a power-law electron distribution and follows its evolution, taking into account the KN cross section, SSC losses, and assuming a blackbody external photon field. The implicit numerical scheme is similar to that used by Chiaberge & Ghisellini (1999) and Graff et al. (2008). After the code reaches a steady state, an increase in the injection rate is introduced that lasts for a short time before it returns to its initial value. The code was initialized to simulate the flare occurring within the BLR and the MT respective, described by the values discussed in Section 2. We assumed a Compton dominance $L_{\mathrm{IC,max}}/L_{\mathrm{synch,max}} \approx 50$, source size $R = 3\times10^{16}$ cm, and bulk Lorentz factor $\Gamma = 10$. Deep in the Thomson regime (MT case) the Compton dominance corresponds to U_{EC}/U_B, where U_{EC} is the external energy density and U_B is the magnetic energy density. However, as cooling transitions from the Thomson to the KN regime (BLR case), the ratio U_{EC}/U_B overestimates the observed Compton dominance by a factor of ∼2.

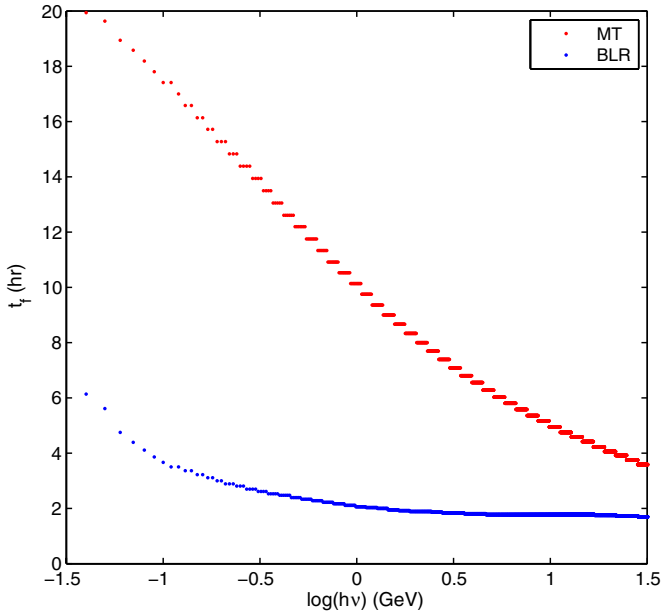

Figure 2. $1/e$ falling time in the galaxy frame vs. observing energy (GeV) for MT seed photons (red) and BLR seed photons (blue).

(A color version of this figure is available in the online journal.)

In the BLR case (Figure 2, blue curve) IC cooling occurs at the onset on the KN regime, resulting in a near-flattening of t_f within the *Fermi* band, where a change in energy by a factor of 100 (from 200 MeV to 20 GeV) results in a change in cooling time of less than an hour, with all the *Fermi* energies having practically indistinguishable decay times (between ∼2–3 hr). In the MT case (Figure 2, red curve) cooling occurs mostly in the Thomson regime and t_f is heavily energy dependent; the same change in energy by a factor of 100 results in a change in cooling time by ∼10 hr. This is also apparent in the light curves shown in Figure 3. A flare occurring within the BLR (Figure 3, top panel) has comparable values of t_f within the *Fermi* energy range. A flare occurring within the MT exhibits distinct falling times that decrease with observing energy (Figure 3, lower panel).

For sufficiently bright flares with short decay times (comparable to the cooling times of a few to several anticipated hours), Fermi light curves can be generated at multiple energies, and the energy dependence (or lack thereof) of t_f can be used to reveal the location of the GeV-emitting site.

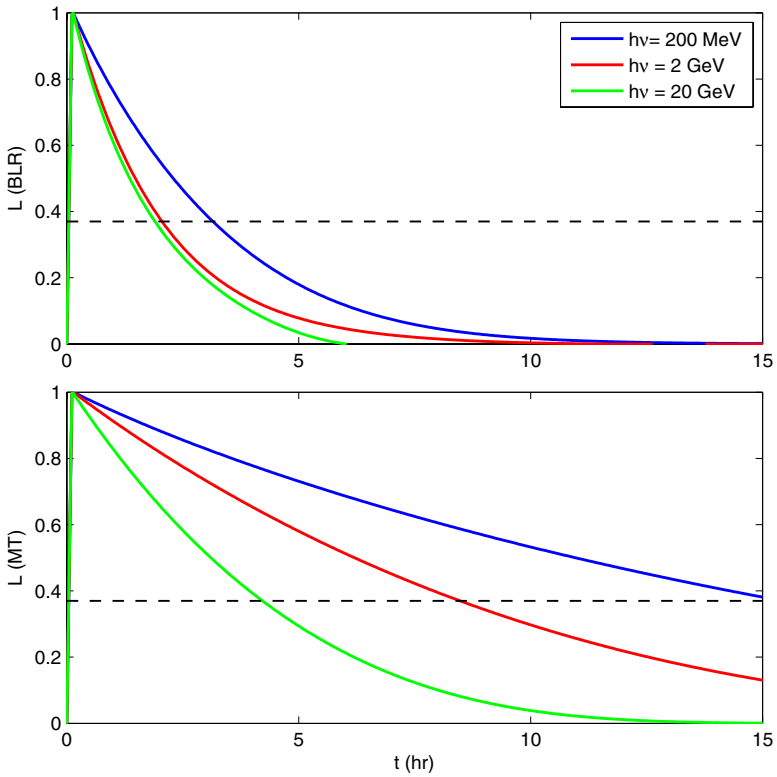

Figure 3. Light curves at 200 MeV, 2 GeV, and 20 GeV for BLR seed photons (upper panel) and MT seed photons (lower panel), normalized for a steady state $L = 0$ and maximum $L = 1$ (in arbitrary units). Times are in the galaxy frame. The dashed black line is the $1/e$ decay time. Times are in the galaxy frame.

(A color version of this figure is available in the online journal.)

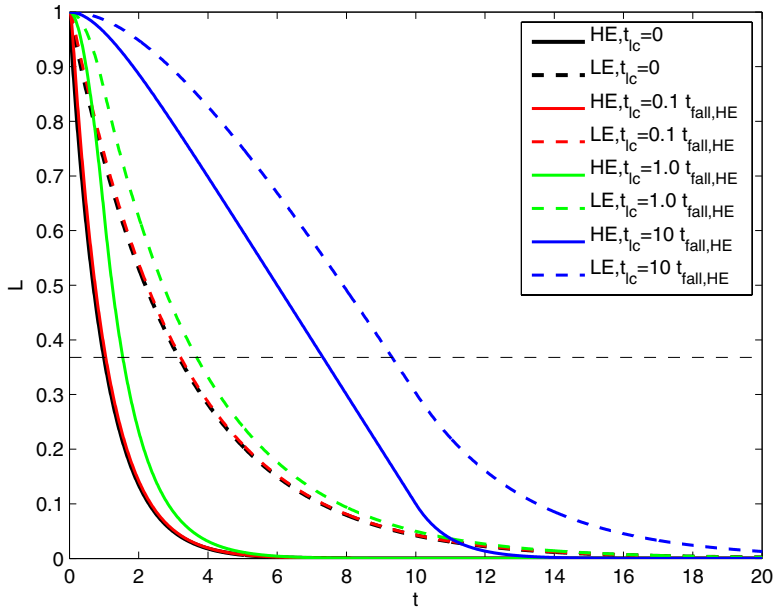

Figure 4. Exponentially decaying light curves of a flare in the MT. High- and low-energy luminosities ($\epsilon_{\rm HE}/\epsilon_{\rm LE} = 10$) are plotted (normalized to 1) for increasing $t_{\rm lc}$. Solid lines represent $\epsilon_{\rm HE}$ and dashed lines $\epsilon_{\rm LE}$. Colors represent $t_{\rm lc}$ at differing factors of t_f, where $t_{f,{\rm HE}}$ is normalized to 1. The dashed black line is the $1/e$ decay time.

(A color version of this figure is available in the online journal.)

3.2. Light-travel Time Effects

Because the GeV emitting region is not a point source, the observed $1/e$ decay time $t_{\rm obs}$ of the light curve is a convolution of t_f and the blob light-crossing time $t_{\rm lc}$. Any other variations (e.g., a gradual decrease of the electron density) will have a similar effect. For BLR achromatic cooling, we expect the light curves to remain achromatic after considering light crossing time effects. To see the effects of $t_{\rm lc}$ in the case of MT cooling, where, $t_f \propto \epsilon^{-1/2}$, we consider a source with an exponentially

decaying emission coefficient, $j(t) = j_0 \exp^{-t/t_f}$, and calculate the expected light curves for two energies differing by 10 and for a range of $t_{\rm lc}$. As can be seen in Figure 4, although $t_{\rm obs}$ increases with increasing $t_{\rm lc}$, the difference of $t_{\rm obs}$ between $\epsilon_{\rm LE}$ and $\epsilon_{\rm HE}$ is practically preserved for all $t_{\rm lc}$. Moreover, because for given $\epsilon_{\rm LE}$ and $\epsilon_{\rm HE}$ the ratio of t_f is also given, observations of the $1/e$ decay times for $\epsilon_{\rm LE}$ and $\epsilon_{\rm HE}$ can be used to find both $t_{\rm lc}$ and t_f for each energy.

3.3. The Feasibility of the Diagnostic

Very bright flares, such as the 2010 November flare of 3C 454.3 (Abdo et al. 2011) have enough photon statistics to produce light curves in two *Fermi* energy bands. The practical application of our diagnostic requires that the decay times in different energy bands have statistically meaningful differences if the flare occurs within the MT. To evaluate if this is the case for a flare as bright as that of 3C 454.3, we adopted the maximum observed errors in the 0.1–1 GeV range and >1 GeV range (Abdo et al. 2011) and produced simulated data assuming energy-dependent cooling in the form of exponentially decaying light curves. We fitted an exponential decay function to the simulated data for each energy band, with the characteristic decay time as a free parameter. The decay times we recovered were statistically distinguishable, suggesting that our diagnostic is applicable, at least for the brightest flares observed.

3.4. Constraints from Upper Limits of the Decay Time Difference

For flares from which no statistically significant difference in the decay time can be established, constraints can still be imposed on the location of the *Fermi*-detected emission by considering $\Delta t_{\rm max}$, the maximum decay time difference allowed by the data, between a high energy $\epsilon_{\rm HE}$ and a low energy $\epsilon_{\rm LE}$. The requirement that $\Delta t_{\rm max} \geqslant t_f(\epsilon_{\rm LE}) - t_f(\epsilon_{\rm HE})$ can be casted as upper limit for the location R of the *Fermi* emission,

$$R \lesssim \left[\frac{2\sigma_T L_{\rm MT} \Gamma^2 \Delta t_{\rm max}}{3\sqrt{3}\,\pi m_e c^2 (1+z)^{1/2} \epsilon_{\rm MT}^{1/2} \left(\epsilon_{\rm LE}^{-1/2} - \epsilon_{\rm HE}^{-1/2}\right)} \right]^{1/2}, \quad (4)$$

where $L_{\rm MT}$ is the MT luminosity. In terms of quantities used in Section 2.1 and for $\epsilon_{\rm LE}$, $\epsilon_{\rm LE}$ corresponding to 100 MeV and 1 GeV, $R \lesssim 2.3 \times 10^{18}\ \Gamma_{10} (\Delta t_{{\rm max},h} L_{{\rm MT},45}/(1+z)^{1/2})^{1/2}$ cm. The Lorentz factor can be estimated from very long baseline interferometry studies (e.g., Jorstad et al. 2005) and the MT luminosity can be taken to be a fraction $\xi \sim 0.1$–0.5 of the accretion disk luminosity or in some cases can be directly measured (e.g., Landt et al. 2010; Malmrose et al. 2011).

4. CONCLUSIONS

We presented a diagnostic test for determining if the GeV emission in powerful blazars originates from within or outside the BLR. Our method utilizes the fact that if electrons cool via IC scattering on BLR photons, cooling occurs at the onset of the KN regime and the resulting cooling times (and thus light curves) should be achromatic. If cooling occurs via IC scattering of less energetic MT photons, the electron cooling times, and thus light curves, should exhibit significant energy dependence and decrease as photon energy increases. The energy dependence of the cooling time difference perseveres in the presence of energy-independent timescales such as the light-crossing time. The method is applicable for the brightest *Fermi* γ-ray flares, and can provide upper limits on the flare location even when the decay times in different energies are statistically indistinguishable.

We thank the referee, Luigi Foschini, for his thoughtful comments and suggestions. We acknowledge support from NASA ATFP grant NNX08AG77G and Fermi grant NNX12AF01G. E.P. and M.G. acknowledge support from LTSA grant NNX07AM17G.

REFERENCES

Abdo, A. A., Ackermann, M., Agudo, I., et al. 2010a, ApJ, 716, 30
Abdo, A. A., Ackermann, M., Ajello, M., et al. 2010b, ApJ, 710, 1271
Abdo, A. A., Ackermann, M., Ajello, M., et al. 2010c, ApJ, 722, 520
Abdo, A. A., Ackermann, M., Ajello, M., et al. 2011, ApJ, 733, L26
Agudo, I., Jorstad, S. G., Marscher, A. P., et al. 2011, ApJ, 726, L13
Aharonian, F., Akhperjanian, A. G., Anton, G., et al. 2009, A&A, 502, 749
Bentz, M. C., Peterson, B. M., Netzer, H., Pogge, R. W., & Vestergaard, M. 2009, ApJ, 697, 160
Błażejowski, M., Sikora, M., Moderski, R., & Madejski, G. M. 2000, ApJ, 545, 107
Blumenthal, G. R. 1971, Phys. Rev. D, 3, 2308
Blumenthal, G. R., & Gould, R. J. 1970, Rev. Mod. Phys., 42, 237
Böttcher, M. 2007, Ap&SS, 309, 95
Chiaberge, M., & Ghisellini, G. 1999, MNRAS, 306, 551
Cleary, K., Lawrence, C. R., Marshall, J. A., Hao, L., & Meier, D. 2007, ApJ, 660, 117
Dermer, C. D. 1995, ApJ, 446, L63
Dermer, C. D., & Atoyan, A. M. 2002, ApJ, 568, L81
Dermer, C. D., & Schlickeiser, R. 1994, ApJS, 90, 945
Dermer, C. D., Schlickeiser, R., & Mastichiadis, A. 1992, A&A, 256, L27
Foschini, L., Ghisellini, G., Tavecchio, F., Bonnoli, G., & Stamerra, A. 2011, A&A, 530, A77
Georganopoulos, M., Kirk, J. G., & Mastichiadis, A. 2001, ApJ, 561, 111
Georganopoulos, M., Perlman, E. S., Kazanas, D., & Wingert, B. 2006, in ASP Conf. Ser. 350, Blazar Variability Workshop II: Entering the GLAST Era, ed. H. R. Miller, K. Marshall, J. R. Webb, & M. F. Aller (San Francisco, CA: ASP), 178
Ghisellini, G., & Tavecchio, F. 2009, MNRAS, 397, 985
Graff, P. B., Georganopoulos, M., Perlman, E. S., & Kazanas, D. 2008, ApJ, 689, 68
Jones, F. C. 1968, Phys. Rev., 167, 1159
Jorstad, S. G., Marscher, A. P., Lister, M. L., et al. 2005, AJ, 130, 1418
Kaspi, S., Brandt, W. N., Maoz, D., et al. 2007, ApJ, 659, 997
Kharb, P., Lister, M. L., & Cooper, N. J. 2010, ApJ, 710, 764
Kishimoto, M., Hönig, S. F., Antonucci, R., et al. 2011, A&A, 527, A121
Kusunose, M., & Takahara, F. 2005, ApJ, 621, 285
Lähteenmäki, A., & Valtaoja, E. 2003, ApJ, 590, 95
Landt, H., Buchanan, C. L., & Barmby, P. 2010, MNRAS, 408, 1982
Malmrose, M. P., Marscher, A. P., Jorstad, S. G., Nikutta, R., & Elitzur, M. 2011, ApJ, 732, 116
Manolakou, K., Horns, D., & Kirk, J. G. 2007, A&A, 474, 689
Maraschi, L., Ghisellini, G., & Celotti, A. 1992, ApJ, 397, L5
Marscher, A. P., Jorstad, S. G., Larionov, V. M., et al. 2010, ApJ, 710, L126
Meyer, E. T., Fossati, G., Georganopoulos, M., & Lister, M. L. 2012, ApJL, 752, L4
Moderski, R., Sikora, M., Coppi, P. S., & Aharonian, F. 2005, MNRAS, 363, 954
Nenkova, M., Sirocky, M. M., Nikutta, R., Ivezić, Ž., & Elitzur, M. 2008, ApJ, 685, 160
Nolan, P. L., Abdo, A. A., Ackermann, M., et al. 2012, ApJS, 199, 31
Poutanen, J., & Stern, B. 2010, ApJ, 717, L118
Sikora, M., Begelman, M., & Rees, M. 1994, ApJ, 421, 153
Sikora, M., Stawarz, Ł., Moderski, R., Nalewajko, K., & Madejski, G. M. 2009, ApJ, 704, 38
Sokolov, A., Marscher, A. P., & McHardy, I. M. 2004, ApJ, 613, 725
Suganuma, M., Yoshii, Y., Kobayashi, Y., et al. 2006, ApJ, 639, 46
Tavecchio, F., & Ghisellini, G. 2008, MNRAS, 386, 945
Tavecchio, F., Ghisellini, G., Bonnoli, G., & Ghirlanda, G. 2010, MNRAS, 405, L94
Zdziarski, A. A. 1989, ApJ, 342, 1108